Research article

Exploration of prognostic and treatment markers in hepatocellular carcinoma via GPCR-related genes analysis

Yuxin Wang, Bao Jin, Xiangan Wu, Jiali Xing, Baoluhe Zhang, Xiaokun Chen, Xiao Liu, Xueshuai Wan, Shunda Du[*]

Department of Liver Surgery, Peking Union Medical College Hospital, Chinese Academy of Medical Sciences and Peking Union Medical College (CAMS & PUMC), Beijing, China

ARTICLE INFO

ABSTRACT

Background: G protein-coupled receptors (GPCRs), the biggest family of signaling receptors, account for 34 % of all the drug targets approved by the Food and Drug Administration (FDA). It has been gradually recognized that GPCRs are of significance for tumorigenesis, but in-depth studies are still required to explore specific mechanisms. In this study, the role of GPCRs in hepatocellular carcinoma (HCC) was elucidated, and GPCR-related genes were employed for building a risk-score model for the prognosis and treatment efficacy prediction of HCC patients.
Methods: Patients' data on HCC were sourced from the Liver Hepatocellular Carcinoma-Japan (LIRI-JP) and The Cancer Genome Atlas (TCGA) databases, while GPCR-related genes were obtained from the Molecular Signatures Database (MSigDB). Univariant and multivariant Cox regression analyses, as well as least absolute shrinkage and selection operator (LASSO) were performed with the aim of identifying differentially expressed GPCR-related genes and grouping patients. Differential expression and functional enrichment analyses were performed; protein-protein interaction (PPI) mechanisms were explored; hub genes and micro ribonucleic acid (miRNA)-target gene regulatory networks were constructed. The tumor immune dysfunction and exclusion (TIDE) algorithm was utilized to evaluate immune infiltration levels and genetic variations. Sensitivity to immunotherapy and common antitumor drugs was predicted via the database Genomics of Drug Sensitivity in Cancer (GDSC).
Results: A GPCR-related risk score containing eight GPCR-related genes (atypical chemokine receptor 3 (ACKR3), C–C chemokine receptor type 3 (CCR3), CCR7, frizzled homolog 5 (FZD5), metabotropic glutamate receptor 8 (GRM8), hydroxycarboxylic acid receptor 1 (HCAR1), 5-hydroxytryptamine receptor 5A (HTR5A) and nucleotide-binding oligomerization domain-like receptor family pyrin domain containing 6 (NLRP6)) was set up. In addition, patients were classified into groups with high and low risks. Patients in the high-risk group exhibited a worse prognosis but demonstrated a more favorable immunotherapy response rate compared with those in the low-risk group. Distinct sensitivity to chemotherapeutic drugs was observed. A clinical prediction model on the basis of GPCR-related risk scores was constructed. Areas under the curves (AUC) corresponding to one-, three- and five-year survival were 0.731, 0.765 and 0.731, respectively.
Conclusions: In this study, an efficient HCC prognostic prediction model was constructed by only GPCR-related genes, which are all potential targets for HCC treatment.

* Corresponding author.
  E-mail address: dushd@pumch.cn (S. Du).

1. Introduction

As the most prevalent and malignant cancer, hepatocellular carcinoma (HCC) accounts for 75%–85 % of primary liver cancer and is considered to be the third major cause of cancer-associated mortality across the globe [1]. Current standard therapeutic strategies encompass maximal surgical resection combined with transarterial chemoembolization, immunotherapy, chemotherapy, molecular targeted therapy, as well as radiotherapy if available. Owning to the inherent heterogeneity of HCC, patients show great differences in their response to immunotherapy and transarterial chemotherapy [2–5]. The prediction and assessment of immunotherapy and chemotherapy sensitivity in HCC patients has long been a prominent area of research interest.

G protein-coupled receptors (GPCRs), which feature a seven-transmembrane receptor with an intracellular C-terminus and an extracellular N-terminus, are the largest superfamily of cell-surface receptors [6]. They serve as essential pivots to communicate between internal and external cellular environments and transduce extracellular signals into intracellular pathways and intricate downstream effectors. Thus, multiple cellular processes are mediated, including sensory, neural, endocrine and immune systems, etc [6]. Given the abundance of druggable sites and their involvement in a wide array of physiological and pathophysiological processes, GPCRs have emerged as highly valuable drug targets and have been the focus of research for decades. Of the current drugs approved by the Food and Drug Administration (FDA), 481 drugs target GPCRs, and take up 34 % of all approved drugs. Currently, approximately 320 GPCR-targeted agents are being clinically tested [7]. Still and all, only less than 15 % of the discovered human GPCRs are targeted and more than half of the non-olfactory GPCRs encoded by genomes remain unexploited in terms of treatment [7]. With breakthroughs in structural biology, the expanded knowledge about the activation of receptors and the application of new methodologies [8], the pace of GPCR research and discovery of GPCR-targeted drugs has accelerated. These concepts lead to new opportunities for the identification of novel GPCR and GPCR-targeted drugs.

About 800 GPCR members have been discovered in humans, and nearly 20 % of human tumors harbor mutations in GPCR-related genes [9,10]. Those mutations are identical in specific tumor types and vary widely among different tumors, which provides the possibility for the application of GPCR-targeted drugs in cancer treatments [9]. Mounting studies have demonstrated that aberrant GPCR expression has a direct relationship with the proliferation, apoptosis, invasion, migration and metastasis of tumor cells, tumor angiogenesis and the formation of the tumor microenvironment [10–13]. Around 70 GPCR somatic mutants were reported in HCC [14] and part of the role played by GPCRs in HCC was also investigated. It was found that some GPCRs exhibited elevated expression levels in HCC compared with normal liver tissues, such as C–C chemokine receptor type 9 (CCR9), chemokine (C-X-C motif) receptor 3 (CXCR3), CXCR6 and G protein-coupled receptor 37 (GPR37). They were linked to tumor number, pathological differentiation and vascular invasion, and could serve as prognostic markers for HCC [15–18]. Some GPCRs were observed to be strongly associated with angiogenesis, including CCR6, CCR7, CXCR2, CXCR7, angiotensin II type 1 receptor (AT1R), AT2R, etc [19–22]. Some were demonstrated to induce epithelial–mesenchymal transition (EMT) and enhance HCC cell migration and invasion, such as CXCR2, CXCR4 and CXCR7 [19,20]. Regarding treatment and drug resistance, leucine-rich repeat-containing G protein-coupled receptor 5 (Lgr5) could lead to doxorubicin resistance in HCC by regulating the programmed cell death protein 5 (PDCD5)/tumor protein 53 (p53) signaling axis [23]. GPCRs were also found to assist in shaping the protumor microenvironment. CXCR6 was demonstrated to up-regulate interleukin-6 (IL-6) and IL-8 and increase the accumulation of neutrophils, which created an inflammatory environment and promoted HCC initiation and invasion [16]. G protein-coupled estrogen receptor (GPER) deficiency could enhance macrophage infiltration and liver fibrosis [24]. CCR4 could mediate regulatory T cells into the tumor microenvironment and promote immune escape in hepatitis B virus (HBV)$^+$HCC [25].

As mentioned above, GPCRs are perfect drug targets and have been demonstrated to play an essential role in HCC development and metastasis, as well as the regulation of the HCC microenvironment. Therefore, we innovatively adopted bioinformatics analysis methods, using large samples from public databases to individually analyze GPCR-related genes in HCC, further exploring the role of GPCR-related genes in predicting the prognosis and treatment sensitivity of HCC. This study can provide a comprehensive and holistic perspective on potential GPCR-related targets and the use of GPCR-related drugs in HCC treatment. With the help of the extensive development of GPCR-related drugs, this study may potentially offer new insights for the treatment of HCC.

Table 1
Baseline information of TCGA-LIHC patients in the TCGA database.

Characteristic	levels	Overall
n		363
Age, n (%)	<60	165 (45.5 %)
	≥60	198 (54.5 %)
Gender, n (%)	female	118 (32.5 %)
	male	245 (67.5 %)
Stage, n (%)	not reported	24 (6.7 %)
	stage I	170 (46.8 %)
	stage II	84 (23.1 %)
	stage III	81 (22.3 %)
	stage IV	4 (1.1 %)

2. Materials and methods

2.1. Data collection

The HCC dataset The Cancer Genome Atlas (TCGA) was provided by University of California, Santa Cruz (UCSC) Xena (https://xena.ucsc.edu). The gene expression sequencing data count and fragments per kilobase million (FPKM) values of patients (n = 424) were downloaded and further normalized to transcripts per million (TPM) values. Meantime, the clinical data of patients were downloaded, such as age, gender, tumor-node-metastasis (TNM) stage, survival time and information on survival status, and patients without clinical information were removed. Finally, 363 samples with complete clinical information were retained. Table 1 shows detailed clinical information. Meanwhile, the mutation data of patients (n = 415) were downloaded from Genomic Data Commons (GDC), selected as "Masked Somatic Mutation" and visualized by use of the maftools R package. In addition, the HCC dataset Liver Hepatocellular Carcinoma-Japan (LIRI-JP) was retrieved and downloaded from the LIRI-JP database, where LIRI-JP contained transcriptomic data for 232 samples and survival data for 260 samples. After the two pieces of information were matched, 232 samples containing survival data were obtained for analysis.

GPCRs bind chemicals in the extracellular environment and activate multiple intracellular signaling pathways, which finally causes cellular changes. A total of 870 GPCR genes were obtained on the basis of the Molecular Signatures Database (MSigDB) (https://www.gsea-msigdb.org/gsea/msigdb/), of which 770 were matched with TCGA and LIRI-JP datasets.

2.2. Subtype analysis of patients with HCC based on GPCR genes

According to TCGA-LIHC expression data and GPCR genes, R package 'ConsensusClusterPlus' [26] was adopted to perform unsupervised clustering analysis and identify GPCR subtypes in HCC patients. This consistent clustering algorithm was utilized for identifying cluster numbers, and the analysis included 1000 iterations to make sure the classification was stable. Principal component analysis (PCA) was performed on patients with grouped subtypes, to see sample differences, and the associations of different subtypes with prognosis were determined using survival analysis.

2.3. GPCR-related prognostic gene screening and risk score model construction

To assess the prognostic value of GPCR genes in HCC patients, a univariate Cox analysis was first used to screen GPCR genes that have a threshold value of P < 0.05. To further identify independent prognostic factors, least absolute shrinkage and selection operator (LASSO) regression [27] and multivariate Cox proportional-hazards models were explored for the screening of independent prognostic factors. A prognostic GPCR-related model was established after 10-fold cross-validation. Below is the computational formula for the risk score.

$$\text{risk}Score = \sum_i Coefficient\ (gene_i) * mRNA\ Expression\ (gene_i)$$

Patients were categorized into groups with high and low risks in accordance with the median of GPCR risk scores. Receiver operating characteristic (ROC) curves were plotted for one, three and five years by time-dependent ROC curves for the purpose of determining accuracy. Additionally, LIRI-JP, an external test set, was used to validate the model. Based on the gene regression coefficients in the model, model accuracy was evaluated by plotting time-dependent ROC curves.

2.4. Analysis of DEGs and functional enrichment in the GPCR-related risk score model

DESeq2 package in R [28] was utilized for identifying DEGs in both groups of HCC patients in TCGA. differentially expressed genes (DEGs) were defined to be genes with adj. *P*-value <0.05 and an absolute value of LogFC >1. Heat and volcano maps were used to visually display the results.

Gene Ontology (GO) analysis [29] is a frequently used approach to performing large-scale research on functional enrichment, including biological processes (BPs), molecular functions (MFs) and cellular components (CCs). Kyoto Encyclopedia of Genes and Genomes (KEGG) [30] is a database widely used for storing information about genomes, drugs, diseases and biological pathways. ClusterProfiler package in R [31] was adopted to conduct GO and KEGG pathway enrichment analyses. It was considered that a critical value of <0.05 for the false discovery rate (FDR) showed statistical significance.

For the purpose of investigating the differences in BPs between all subgroups, GSEA [32] was used to perform a gene set enrichment analysis based on the HCC patients' gene expression profile dataset. As a computational method of analyzing the statistical difference between two biological states in a particular gene set, GSEA is frequently used for estimating the pathway and changes in BP activity. The effect of groups with high and low risks on tumor KEGG was assessed by downloading the "c2.cp.kegg.symbols.gmt" gene set from the MSigDB database for GSEA. FDR <0.25 was taken into account in the results.

2.5. Protein-protein interaction (PPI) and regulatory networks

The STRING database [33] was used to analyze the interactions between DEG-encoded proteins, and the results were exported to further screen hub genes through the plugin CytoHubba in Cytoscape. Based on the prediction of the mirTarbse database (https://

mirtarbase.cuhk.edu.cn/), possible regulatory micro ribonucleic acids (miRNAs) were predicted based on the evidence of "luciferase reporter gene assay", and related long non-coding RNAs (lncRNAs) were further predicted. The Cytoscape software was used to visualize the results of competitive endogenous RNA (ceRNA) analysis.

2.6. Identification and correlation analysis of tumor immune infiltrating cells

The estimation of stromal and immune cells in malignant tumor tissues using the expression data (ESTIMATE) package for R [34] was used to assess the immunoreactivity of the tumor microenvironment. ESTIMATE analysis quantified immunoreactivity (immune infiltration level) in tumor samples based on gene expression profiles, and an immune score was obtained for each tumor sample. A comparison was made between the differences in the immune infiltration characteristics of patients with HCC in both groups.

To clarify the specific infiltration level of immune cells, the CIBERSORT algorithm [35] was used for deconvoluting the HCC transcriptome expression matrix, which thus estimated immune cell composition and abundance in mixed cells. Data of the gene expression matrix were uploaded to CIBERSORT, and the output of samples with $p < 0.05$ was filtered to obtain the matrix of immune cell infiltration. The ggplot2 package in R was used to draw histograms showing how 22 immune cell infiltrates were distributed in each sample.

2.7. Analysis of single nucleotide polymorphisms and copy number variation

Maftools package was utilized for analyzing the high-frequency mutated genes of patients in groups with high and low risks to analyze single nucleotide polymorphisms (SNPs). Then, the Masked Copy Number Segment data were downloaded through GDC. The analysis of the downloaded copy number variation (CNV) segments was completed by GenePattern with Genomic Identification of Significant Targets in Cancer (GISTIC) 2.0. GISTIC 2.0 analysis was performed using default parameters.

2.8. TMB, MSI and predictive analysis of tumor immunotherapy response

The maftools R package was used to calculate the data on the TMB of HCC patients. MSI-Sensor data were gathered from the cBioportal database (https://www.cbioportal.org). The underlying tumor treatment response of immune checkpoint blockade (ICB) was predicted by the tumor immune dysfunction and exclusion (TIDE) score [36], a computational algorithm based on gene expression profiles (http://tide.dfci.harvard.edu). Differences between both groups were compared with the TIDE analysis results.

2.9. Analysis of drug sensitivity

The database GDSC (www.cancerrxgene.org/) [37] was utilized for finding data on oncology drug response and sensitive genome markers. The pRRophetic algorithm [38] was used for the construction of a ridge regression model on the basis of gene expression profiles to forecast the sensitivity of high- and low-risk groups to commonly used anticancer drugs by half maximal inhibitory concentration (IC50) values. Moreover, common oncological chemotherapeutic agents were extracted, including cisplatin, etoposide, paclitaxel, cyclophosphamide, etc. Differences in chemotherapeutic drug sensitivity between different subgroups were clarified.

2.10. Clinical prognosis prediction model construction based on GPCR risk scores

The individualized evaluation of GPCR risk scores in combination with the clinicopathological characteristics of patient prognosis was demonstrated by performing a multivariant Cox analysis and constructing a nomogram. The predicted values of the model were compared with the actual observed survival to generate calibration curves and assess performance. Based on the rms R package (https://cran.r-project.org/web/packages/rms/), the model was resampled 1000 times using the bootstrap method to ensure that the nomogram was accurate.

2.11. Statistical analysis

R software (version 4.1.3) was used to perform all data processing and analysis. To compare the continuous variables of both groups, independent Student t-tests were used to estimate whether normally distributed variables were statistically significant. Additionally, the Mann-Whitney U test (i.e. Wilcoxon rank sum test) was utilized to analyze the differences between non-normally distributed variables. A chi-square or Fisher exact test was utilized for comparing and analyzing whether the categorical variables of both groups were statistically significant. Survival analysis was performed using the survivor package of R. Survival differences were shown using Kaplan-Meier (KM) survival curves. A log-rank test was utilized to assess whether both groups showed significant differences in survival time. Then, pROC package in R was applied to plot time-dependent ROC curves, and the calculation of areas under the curve (AUCs) [39] was conducted to evaluate the accuracy of risk scores and thus estimate prognosis. Each statistical P value was two-sided and showed statistical significance at $P < 0.05$.

3. Results

3.1. Expression and mutational alterations of GPCR-associated genes in HCC patients

The research workflow is shown in Fig. 1. First, 770 GPCR-related genes were extracted from the RNA-sequencing (RNA-seq) data of TCGA-LIHC, and a comparison was made between the expression differences of HCC and normal liver tissues. After a univariant Cox regression analysis, 38 of these 770 GPCR-related genes were observed to be differentially expressed, and almost all of them were overexpressed in HCC (Fig. 2A), which suggested that these genes may play an essential role in HCC tumorigenesis. Then, the mutation information of those 38 GPCR-related genes was extracted by maftools package, and their SNP mutation frequencies were found to be generally low (Fig. 2B). The above results revealed that these GPCR-related genes may play a major role at the transcriptional or post-transcriptional level.

3.2. Identification of HCC GPCR subtypes

On the basis of the above DEGs related to GPCRs, consistent clustering was used for the clustering of HCC samples. When k = 2, the best clustering distribution was obtained, and subgroups 1 and 2 were identified (Fig. 2C and D). HCC transcriptome data were downscaled by PCA, and principal components PC1 and PC2 were obtained. The PCA results of the two groups were plotted, and it was found that both groups were clearly distinguished (Fig. 2E). After that, the prognostic characteristics of the two subgroups were analyzed by KM curves, but the results revealed no significant prognostic differences (Fig. 2F). The above results suggested that differentially expressed GPCR-related genes could well guide the subtyping of HCC patients. Nevertheless, subtyping could not yet assess prognostic differences.

3.3. Construction and evaluation of GPCR-related risk scores

LASSO and multivariant Cox regression analyses were performed among 38 genes (Fig. 3A and B). Eight genes with the optimal prognostic value were obtained, namely atypical chemokine receptor 3 (ACKR3), CCR3, CCR7, frizzled homolog 5 (FZD5), metabotropic glutamate receptor 8 (GRM8), hydroxycarboxylic acid receptor 1 (HCAR1), 5-hydroxytryptamine receptor 5A (HTR5A) and nucleotide-binding oligomerization domain-like receptor family pyrin domain containing 6 (NLRP6) (Fig. 3C). Meanwhile, the coefficients of key characteristic genes computed by the multivariate Cox analysis were obtained. Gene expression was multiplied with corresponding coefficients and summed to set up a GPCR-related risk score. The final risk scores of all samples were calculated.

$$riskScore = ACKR3 \times 0.213 + CCR3 \times 0.386 + CCR7 \times 0.409 + FZD5 \times 0.201 + GRM8 \times 0.295 + HCAR1 \times 0.689 + HTR5A$$
$$\times 0.866 - NLRP6 \times 0.268$$

Patients were divided into groups with high and low risks on the basis of the median expression values of risk scores in the TCGA dataset, and a heatmap was plotted (Fig. 3D). KM curves demonstrated a significantly worse prognosis in the high-risk group of patients and a great difference in survival between high- and low-risk groups of patients (p < 0.001) (Fig. 3E). Additionally, time-
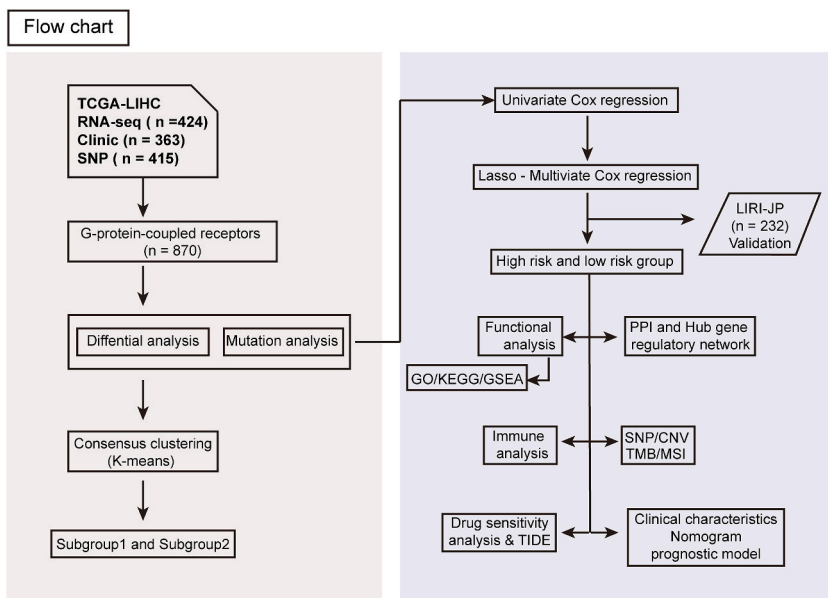
Fig. 1. Flow chart of the whole research work.
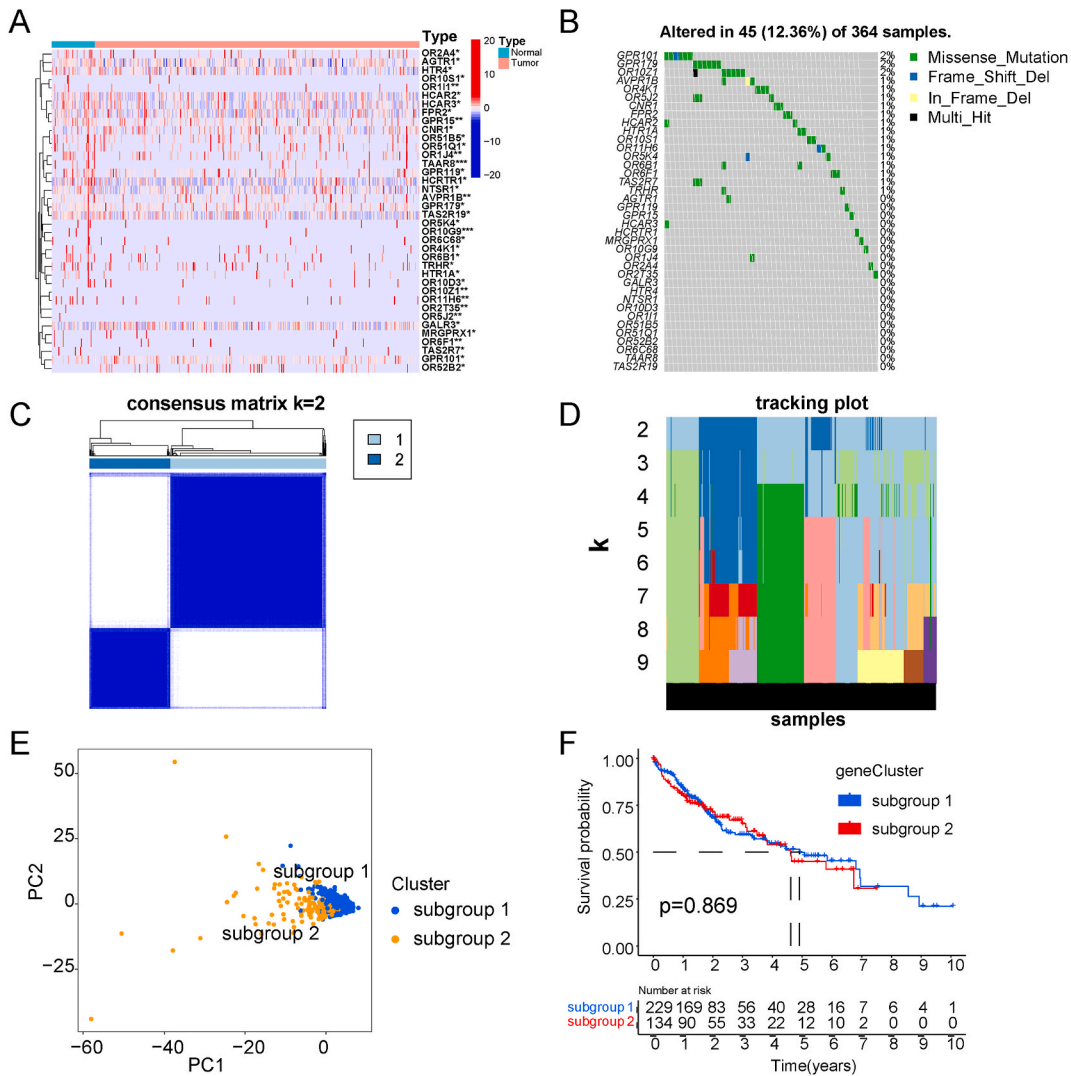
Fig. 2. Differential expression of GPCR genes and the identification of subtypes in TCGA-LIHC patients. (A) Differential expression of GPCR genes in tumor and tumor groups. (B) Alternation in the somatic mutation of GPCR genes in the group with LIHC patients. (C) Heatmap of K = 2 sample clustering by use of consistent clustering. (D) The plot of sample tracking when K = 2–9, where different colors stand for the distribution of various cluster samples, and vertical and horizontal coordinates represent K values and samples, respectively. (E) PCA plot for subgroups 1 and 2. (F) KM method for comparing the difference between subgroups 1 and 2 in survival; both subtypes of patients were not statistically and significantly different. (For interpretation of the references to color in this figure legend, the reader is referred to the Web version of this article.)

dependent ROC curve analysis demonstrated that the risk score had excellent predictive power for the overall survival (OS) of HCC patients, where AUCs were 0.804, 0.787 and 0.750 for one-, three- and five-year OS, respectively (Fig. 3E). In the external validation dataset LIRI-JP, the high-risk group of patients were also found to have a significantly worse prognosis (p < 0.01), and ROC curves had an AUC of 0.764, 0.704 and 0.746 for one-, three- and five-year OS, respectively. This indicated that the model performed well in the external dataset as well (Fig. 3F).

3.4. Analysis of DEGs in patients with GPCR-related risk scores in high- and low-risk groups

To analyze the association between GPCR-related risk scores and HCC development, PCA was explored and plots demonstrated an obvious distinction between both groups of patients (Fig. 4A). Later, a differential expression analysis was conducted on both groups of patients. The results showed that 1976 significant DEGs were obtained, including 1371 up-regulated DEGs and 605 down-regulated DEGs (Fig. 4B and C).

Next, a functional enrichment analysis was performed on these 1976 DEGs. The GO analysis suggested that DEGs were associated with nuclear division, mitotic nuclear division and mitotic sister chromatid segregation in BPs. In addition, they were related to synaptic and basolateral plasma membranes, kinesin complex and condensed nuclear chromosome kinetochore in CCs, and substrate-
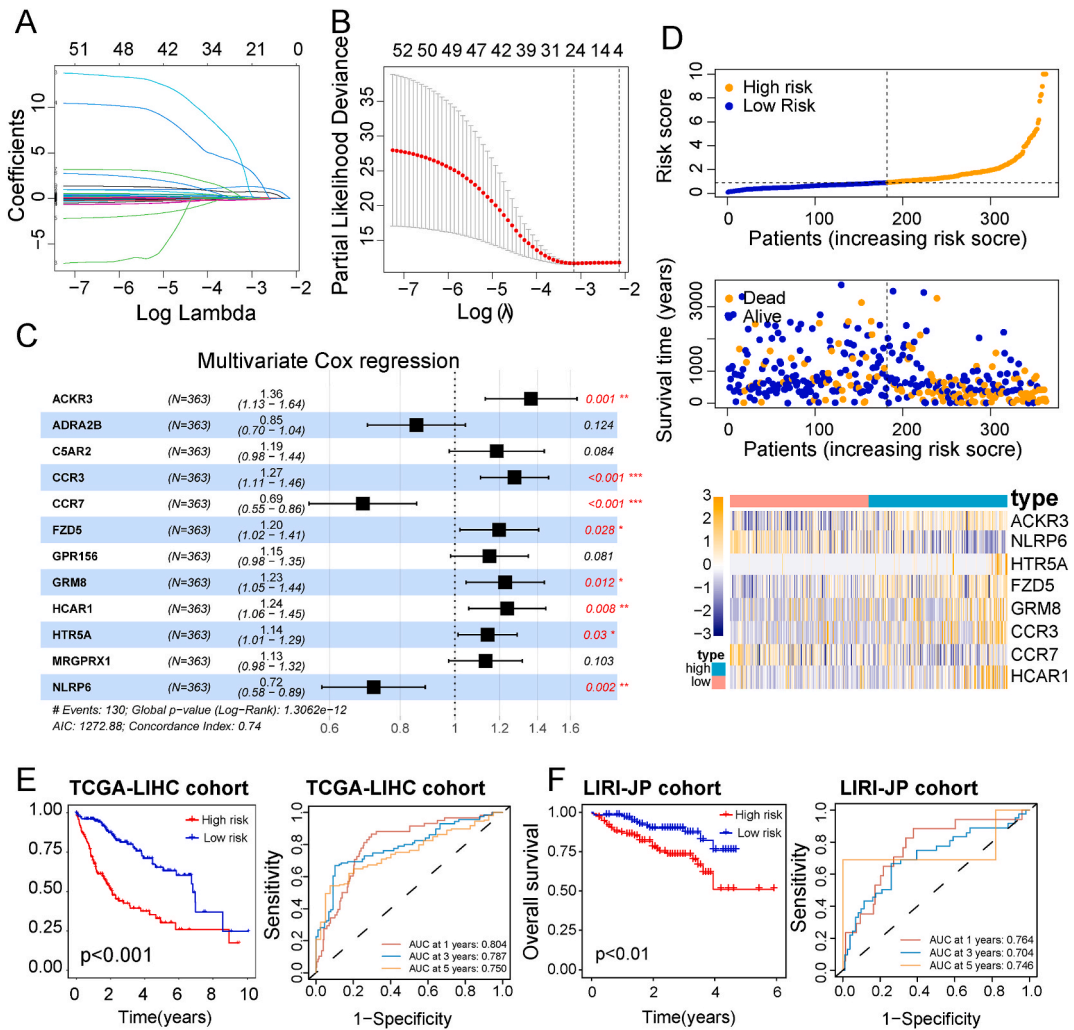
Fig. 3. GPCR-related risk score model construction. (A–B) LASSO regression analyses with the best lamda value corresponding to the number of seven variables. (C) Results of multifactorial Cox stepwise regression (direction = "both") analysis; eight genes were finally identified as independent prognostic factors. (D) Risk score distribution, patient survival and heatmap of characteristic gene expression in LIHC patients. (E) The left side is the KM curve of patients in both groups in the training dataset, which demonstrates a greatly worse prognosis in the high-risk group of patients; the right side shows the time-dependent ROC curve of TCGA-LIHC patients. (F) The left side is the KM curve of patients in both groups in the validation dataset LIRI-JP, which indicates a greatly worse prognosis in high-risk group patients; the right side shows the time-dependent ROC curve analysis of LIRI-JP.

specific channel, channel, passive transmembrane transporter and ion channel activities in MFs (Fig. 4D). The KEGG functional analysis results indicated that DEGs principally affect bile secretion and neuroactive ligand- and extracellular matrix (ECM)-receptor interactions (Fig. 4E). Tables 2 and 3 show detailed GO and KEGG results.

GSEA was further explored, and the results of the pathway database were summarized on the basis of the KEGG results. The results showed the significant enrichment of fatty acid, glycine, serine, threonine and retinol metabolism, primary bile acid biosynthesis and other hallmarks in the group with high risk (Fig. 5A). Additionally, the results indicated the significant enrichment of ECM- and neuroactive ligand-receptor interactions, o-glycan biosynthesis and cell cycle in the group with low risk (Fig. 5B). Table 4 presents the detailed GSEA results of metabolism-associated pathways.

3.5. Analysis of PPI and regulation networks

Hub genes playing a key role were further clarified, and an attempt was made to reveal their potential molecular interaction mechanisms. The STRING database was used for analyzing the PPI mechanism. It can be seen from Fig. 6A that the number of PPI nodes (proteins) was 38 after confidence = 0.400 screening; the number of linkages (edges) was 48; the average connectivity per node was 2.53; the whole PPI had an enrichment statistic P value of below 1.0e-16.
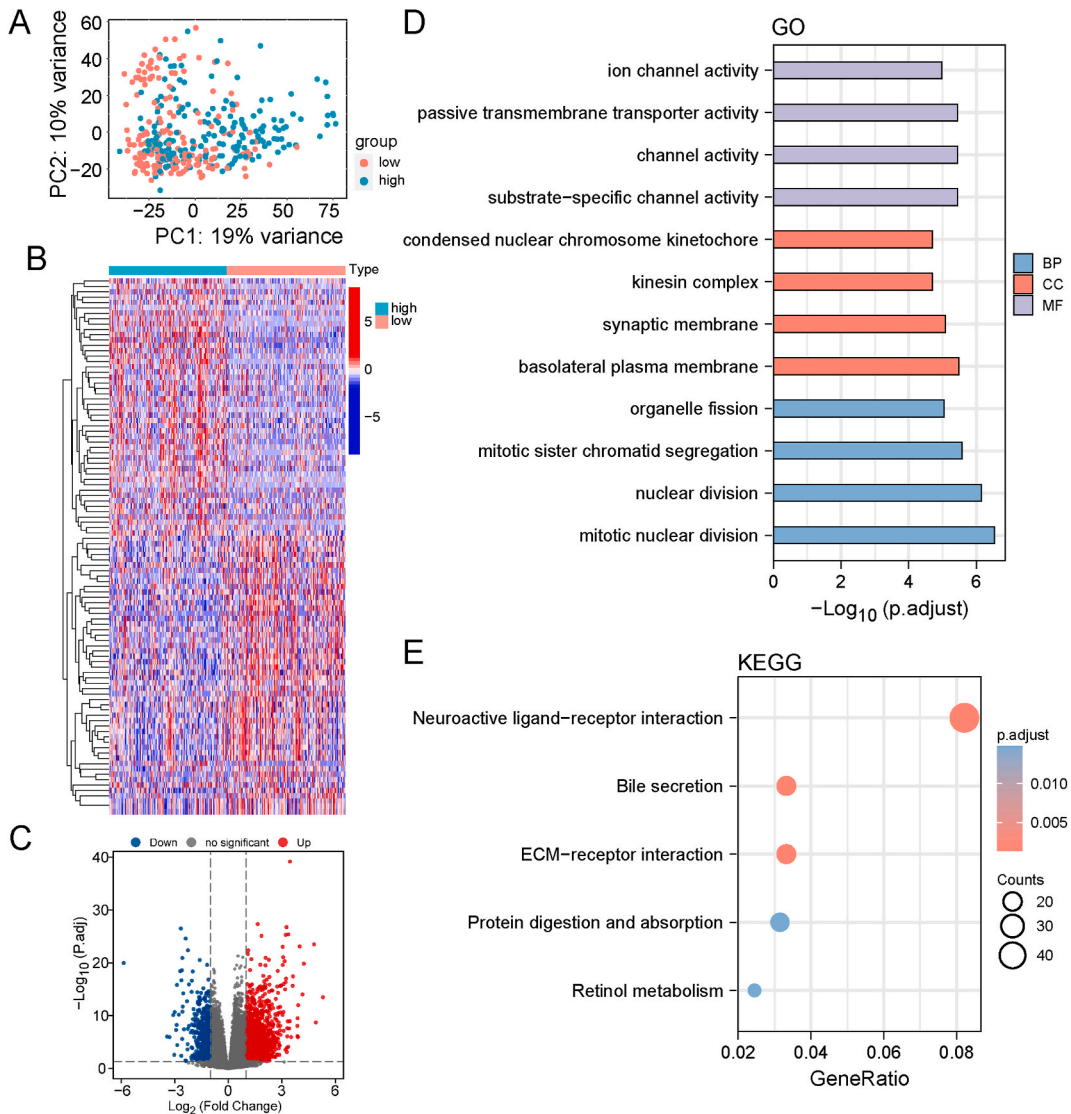
Fig. 4. DEG and functional enrichment analyses on the basis of the GPCR-related risk score model. (A) PCA plots of the overall differences between the high and low-risk groups of TCGA. (B–C) Volcano and heatmap demonstrating the expression of DEGs between LIHC patients with high and low risks in the TCGA dataset. (D) GO analysis results between TCGA-LIHC patients in both groups. (E) KEGG analysis results between TCGA-LIHC patients in both groups.

Afterwards, the plugin CytoHubba in Cytoscape was utilized for further clarifying the proteins in which interactions occur to serve as hub genes. After calculation, it was found that GPR119, cannabinoid receptor 1 (CNR1), arginine vasopressin receptor 1B (AVPR1B), 5-hydroxytryptamine receptor 1A (HTR1A) and thyrotropin-releasing hormone receptor (TRHR) were the highest scoring interacting proteins (Fig. 6B). After that, miRNA molecules potentially regulating these hub genes were analyzed using the mirTarbase database, and Cytoscape was employed for constructing miRNA-target gene regulatory networks (Fig. 6C).

3.6. Immune infiltration analysis of groups with high and low risks

Next, the associations of GPCR-related risk scores with the level of different immune cell infiltrates and overall immune characteristics in HCC patients were evaluated. When a comparison was made between the immune cell infiltration in groups with high and low risks, it was found that only naive B cells were significantly different in both groups, but any other immune cells were not statistically and significantly different (Fig. 7A). The analysis of correlation between immune cells showed that macrophages, monocytes and B cells accountable for antigen presentation were not significantly correlated with CD4 and CD8 T cells responsible for killing (Fig. 7B). According to the ESTIMATE results, groups with high and low risks were statistically and significantly different in the cellular infiltration level of the tumor microenvironment and immune correlation scores; the immune and stromal cell infiltration of the high-

Table 2
Top 20 significant genes in GO analysis.

ONTOLOGY	ID	Description	GeneRatio	pvalue	qvalue	Count
BP	GO:0140014	mitotic nuclear division	51/1334	5.5297E-11	2.6409E-07	51
BP	GO:0000280	nuclear division	66/1334	2.6889E-10	6.4208E-07	66
BP	GO:0000070	mitotic sister chromatid segregation	34/1334	1.4812E-09	2.3579E-06	34
BP	GO:0048285	organelle fission	67/1334	6.7362E-09	8.0427E-06	67
BP	GO:1902850	microtubule cytoskeleton organization involved in mitosis	30/1334	8.8873E-09	8.4888E-06	30
BP	GO:0000819	sister chromatid segregation	37/1334	1.6462E-08	1.301E-05	37
BP	GO:0007052	mitotic spindle organization	26/1334	1.9069E-08	1.301E-05	26
BP	GO:0030198	extracellular matrix organization	57/1334	2.4111E-08	1.4394E-05	57
BP	GO:0007059	chromosome segregation	50/1334	1.4519E-07	7.7043E-05	50
BP	GO:0043062	extracellular structure organization	60/1334	2.3461E-07	0.00010762	60
BP	GO:0098813	nuclear chromosome segregation	43/1334	2.4788E-07	0.00010762	43
BP	GO:0051783	regulation of nuclear division	34/1334	4.4798E-07	0.00017829	34
BP	GO:0048562	embryonic organ morphogenesis	45/1334	5.5201E-07	0.00020279	45
BP	GO:0099177	regulation of *trans*-synaptic signaling	60/1334	7.7998E-07	0.00024928	60
BP	GO:0016266	O-glycan processing	17/1334	7.8294E-07	0.00024928	17
BP	GO:0048568	embryonic organ development	59/1334	8.4259E-07	0.0002515	59
BP	GO:0042445	hormone metabolic process	38/1334	1.2818E-06	0.00036009	38
BP	GO:0050804	modulation of chemical synaptic transmission	59/1334	1.5535E-06	0.00039072	59
BP	GO:0051480	regulation of cytosolic calcium ion concentration	51/1334	1.6155E-06	0.00039072	51
BP	GO:0007088	regulation of mitotic nuclear division	30/1334	1.6362E-06	0.00039072	30
CC	GO:0016323	basolateral plasma membrane	41/1391	5.8276E-09	2.6868E-06	41
CC	GO:0097060	synaptic membrane	63/1391	2.9299E-08	6.7541E-06	63
CC	GO:0005871	kinesin complex	17/1391	1.2539E-07	1.6497E-05	17
CC	GO:0000778	condensed nuclear chromosome kinetochore	9/1391	1.4313E-07	1.6497E-05	9
CC	GO:0000779	condensed chromosome, centromeric region	25/1391	5.8004E-07	4.3583E-05	25
CC	GO:0000775	chromosome, centromeric region	34/1391	6.3612E-07	4.3583E-05	34
CC	GO:0098793	presynapse	65/1391	6.617E-07	4.3583E-05	65
CC	GO:0000793	condensed chromosome	37/1391	9.553E-07	5.5056E-05	37
CC	GO:0000940	condensed chromosome outer kinetochore	8/1391	1.2298E-06	6.2999E-05	8
CC	GO:0000776	kinetochore	26/1391	2.36E-06	0.00010881	26
CC	GO:0099572	postsynaptic specialization	49/1391	2.77E-06	0.00011553	49
CC	GO:0098978	glutamatergic synapse	49/1391	3.0069E-06	0.00011553	49
CC	GO:0000777	condensed chromosome kinetochore	22/1391	3.2962E-06	0.0001169	22
CC	GO:1902495	transmembrane transporter complex	46/1391	4.4261E-06	0.00014576	46
CC	GO:0000780	condensed nuclear chromosome, centromeric region	10/1391	5.515E-06	0.00016951	10
CC	GO:0016324	apical plasma membrane	45/1391	6.1116E-06	0.00017611	45
CC	GO:0034702	ion channel complex	43/1391	7.6656E-06	0.00019618	43
CC	GO:0042734	presynaptic membrane	28/1391	7.7805E-06	0.00019618	28
CC	GO:0005604	basement membrane	20/1391	8.4264E-06	0.00019618	20
CC	GO:1990351	transporter complex	46/1391	8.51E-06	0.00019618	46
MF	GO:0022838	substrate-specific channel activity	66/1314	1.0166E-08	3.1517E-06	66
MF	GO:0015267	channel activity	69/1314	1.0332E-08	3.1517E-06	69
MF	GO:0022803	passive transmembrane transporter activity	69/1314	1.1313E-08	3.1517E-06	69
MF	GO:0005216	ion channel activity	63/1314	4.3919E-08	9.1768E-06	63
MF	GO:0008509	anion transmembrane transporter activity	52/1314	1.3809E-07	2.3083E-05	52
MF	GO:0022836	gated channel activity	52/1314	6.3595E-07	7.6378E-05	52
MF	GO:0046873	metal ion transmembrane transporter activity	62/1314	6.3969E-07	7.6378E-05	62
MF	GO:0022839	ion gated channel activity	49/1314	3.4496E-06	0.00036039	49
MF	GO:0005261	cation channel activity	46/1314	1.0766E-05	0.00099982	46
MF	GO:0008017	microtubule binding	38/1314	1.2906E-05	0.00107865	38
MF	GO:0008514	organic anion transmembrane transporter activity	34/1314	1.4699E-05	0.00111687	34
MF	GO:1901618	organic hydroxy compound transmembrane transporter activity	12/1314	6.0364E-05	0.00420433	12
MF	GO:0008146	sulfotransferase activity	13/1314	8.0923E-05	0.00499379	13
MF	GO:0015631	tubulin binding	45/1314	8.3649E-05	0.00499379	45
MF	GO:0003777	microtubule motor activity	17/1314	0.00012412	0.0069158	17
MF	GO:0005201	extracellular matrix structural constituent	26/1314	0.00016952	0.00885503	26
MF	GO:0004222	metalloendopeptidase activity	19/1314	0.00018593	0.00903072	19
MF	GO:0005249	voltage-gated potassium channel activity	17/1314	0.00019449	0.00903072	17
MF	GO:0005267	potassium channel activity	21/1314	0.00026951	0.01185541	21
MF	GO:0022843	voltage-gated cation channel activity	23/1314	0.00031315	0.01308632	23

risk group was significantly lower than that of the low-risk group; the high-risk group exhibited higher tumor purity than the low-risk one (Fig. 7C). Further, the correlation of patients' risk scores with immune cells was compared. It was discovered that risk scores presented a positive trend with cells like M0 macrophages and memory B cells and a negative trend with M1 macrophages, CD8 T and naive B cells, etc. Nonetheless, the degree of these correlations was low and not statistically significant (Fig. 7D). Subsequently, a comparison was made between the expression of immune checkpoint-related genes in both groups. It was noted that a number of important immune checkpoint genes, including a cluster of differentiation 8a (CD8A), hepatitis A virus cellular receptor 2 (HAVCR2),

Table 3
KEGG analysis results.

ONTOLOGY	ID	Description	GeneRatio	BgRatio	pvalue
KEGG	hsa04080	Neuroactive ligand-receptor interaction	47/572	341/8076	6.3794E-06
KEGG	hsa04512	ECM-receptor interaction	19/572	88/8076	9.2739E-06
KEGG	hsa04976	Bile secretion	19/572	90/8076	1.3074E-05
KEGG	hsa00830	Retinol metabolism	14/572	68/8076	0.00023607
KEGG	hsa04974	Protein digestion and absorption	18/572	103/8076	0.00028894
KEGG	hsa04911	Insulin secretion	16/572	86/8076	0.00029839
KEGG	hsa04110	Cell cycle	20/572	124/8076	0.00040995
KEGG	hsa05030	Cocaine addiction	11/572	49/8076	0.00050003
KEGG	hsa04060	Cytokine-cytokine receptor interaction	35/572	295/8076	0.00167833
KEGG	hsa04918	Thyroid hormone synthesis	13/572	75/8076	0.00211463
KEGG	hsa04724	Glutamatergic synapse	17/572	114/8076	0.002612
KEGG	hsa04024	cAMP signaling pathway	27/572	216/8076	0.00264907
KEGG	hsa00591	Linoleic acid metabolism	7/572	29/8076	0.00340721
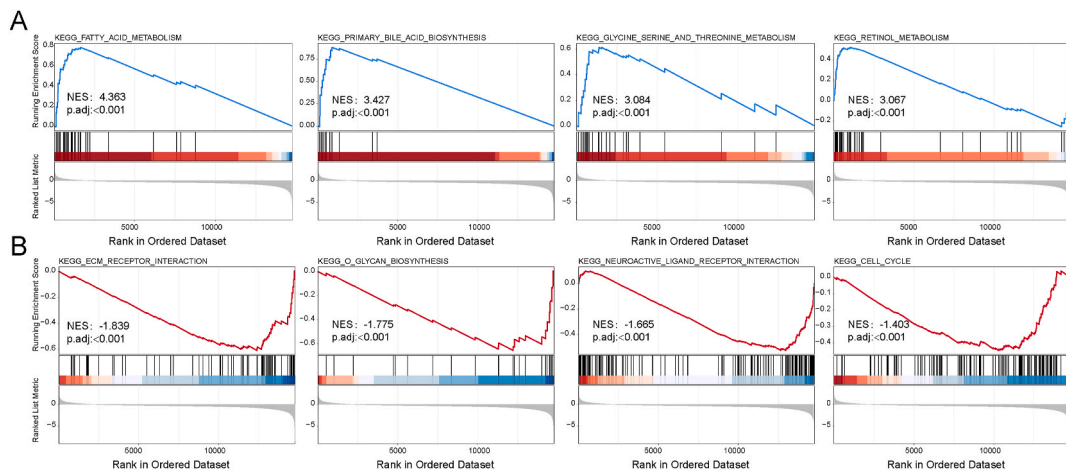
Fig. 5. GSEA analysis. (A) Significant enrichment of primary bile acid biosynthesis, fatty acid, glycine, serine, threonine and retinol metabolism, etc. in the high-risk group. (B) Significant enrichment of ECM- and neuroactive ligand-receptor interactions, o-glycan biosynthesis, cell cycle, etc. in the low-risk group.

chemokine (C-X-C motif) ligand 10 (CXCL10), CXCL9, Perforin 1 (PRF1), etc., were differentially expressed in both groups (Fig. 7E). The above results suggested that GPCR risk scores were not significantly associated with the tumor microenvironment, which highly indicated that the expression of GPCR-related DEGs mainly affects the changes in the tumor itself and has less effect on immune or stromal cells.

3.7. Effect of GPCR-related risk scores on genomic changes in HCC patients

Later, the effect of GPCR-related risk scores on changes in the level of genetic variation was further evaluated, like SNPs and CNVs. The SNP mutation analysis results of driver genes in common tumorigenesis revealed that both groups of patients demonstrated similar mutation levels (Fig. 8A-B). In the comparison of TMB and MSI, TMB showed no significant difference (Fig. 8C), while MSI exhibited an elevation in the high-risk group (Fig. 8D). The study of CNV alteration frequency showed widespread CNV in both groups of patients but was not significantly different (Fig. 8E-F).

3.8. Differences in drug sensitivity between both groups of patients

Then, the sensitivity phenotypes of commonly used antitumor drugs between groups with high and low risks were evaluated via the GDSC database. Firstly, GDSC data were taken as a training set, and the pRRophetic package was used to construct a ridge regression model. After that, the data of the TCGA-LIHC dataset were input for testing. As revealed by the test results, 51 out of 138 input drugs were observed to show statistical differences between both groups. Then, boxplots were used to plot the six most statistically different drugs and small molecule compounds. Among these drugs and small molecule compounds, BIRB.0796 and all-trans retinoic acid (ATRA) showed higher sensitivity to the high-risk group of patients, while AZD8055, EHT.1864, PF.4708671 and GW.441756 showed higher sensitivity to the low-risk group of patients (Fig. 9A–F).

Considering that immunotherapy plays a vital part in HCC treatment currently, the TIDE algorithm was adopted to evaluate the

Table 4
GSEA analysis results.

ID	setSize	NES	p.adjust	qvalue
KEGG_FATTY_ACID_METABOLISM	39	4.362864	8.75E-09	7.00E-09
KEGG_PRIMARY_BILE_ACID_BIOSYNTHESIS	16	3.427042	8.75E-09	7.00E-09
KEGG_RETINOL_METABOLISM	49	3.066979	1.42E-07	1.14E-07
KEGG_GLYCINE_SERINE_AND_THREONINE_METABOLISM	29	3.084273	2.24E-06	1.79E-06
KEGG_PRIMARY_IMMUNODEFICIENCY	25	3.061342	4.80E-06	3.84E-06
KEGG_NEUROACTIVE_LIGAND_RECEPTOR_INTERACTION	143	−1.66461	3.12E-05	2.50E-05
KEGG_VALINE_LEUCINE_AND_ISOLEUCINE_DEGRADATION	39	2.542273	8.39E-05	6.71E-05
KEGG_ECM_RECEPTOR_INTERACTION	66	−1.8386	8.58E-05	6.86E-05
KEGG_LINOLEIC_ACID_METABOLISM	22	2.678666	0.000336	0.000269
KEGG_TRYPTOPHAN_METABOLISM	32	2.503453	0.000414	0.000331
KEGG_PROPANOATE_METABOLISM	27	2.385105	0.001341	0.001073
KEGG_BUTANOATE_METABOLISM	28	2.401353	0.001459	0.001167
KEGG_TYROSINE_METABOLISM	30	2.27098	0.002981	0.002385
KEGG_RENIN_ANGIOTENSIN_SYSTEM	14	2.110067	0.008246	0.006597
KEGG_STEROID_HORMONE_BIOSYNTHESIS	43	1.985456	0.012971	0.010377
KEGG_ASTHMA	15	1.965837	0.015989	0.012791
KEGG_O_GLYCAN_BIOSYNTHESIS	23	−1.77524	0.015989	0.012791
KEGG_BETA_ALANINE_METABOLISM	20	2.002323	0.021878	0.017502
KEGG_HISTIDINE_METABOLISM	25	1.977649	0.026026	0.02082
KEGG_PROTEASOME	37	1.8651	0.026026	0.02082
KEGG_DRUG_METABOLISM_OTHER_ENZYMES	47	1.840722	0.026026	0.02082
KEGG_CELL_CYCLE	121	−1.40341	0.029283	0.023427
KEGG_SYSTEMIC_LUPUS_ERYTHEMATOSUS	42	1.811271	0.045285	0.036228
KEGG_ARACHIDONIC_ACID_METABOLISM	45	1.765372	0.045285	0.036228

sensitivity of patients in both groups to immunotherapy. As shown in Fig. 9G–I, the high-risk group exhibited lower TIDE scores than the low-risk one, which indicated that patients in the high-risk group might have better responsiveness to immunotherapy than those in the low-risk group. Dysfunction and exclusion scores were combined, which demonstrated immune dysfunction and possibly stronger immune escape in the group with high risk. Through the combination of previous analyses that the high-risk group exhibited an MSI score, it was inferred that the responsiveness of patients in the group with high risk to immunotherapy might be better.

3.9. Clinical prediction model construction based on GPCR-associated risk scores

To further examine the potential clinical significance of GPCR-associated risk scores, the composition of gender, age and TNM stage among both groups of patients in the TCGA-LIHC dataset was analyzed first. It was noticed that the age and gender composition of patients in both groups were not significantly different, but the results of the staging comparison demonstrated that the low-risk group had a higher proportion of stage I patients than the high-risk one (Fig. 10A–C).

Subsequently, a prognostic model was built based on the GPCR-associated risk scores and clinicopathological features (gender, age and TNM stage) of HCC patients and visualized in the nomogram (Fig. 10D). Calibration curves were used for assessing model accuracy, and the modeled one-, three- and three-year OS estimates were found to well agree with the actual observations of patients (Fig. 10E).

4. Discussion

Systemic therapy benefits a small proportion of patients despite having made significant advancements and playing an increasingly crucial role in treating HCC. The lack of direct targets may be one of the reasons for low response rates, which thus makes it critical to identify potential target drugs. GPCRs, the most prominent drug targets among FDA-approved drugs, have played a significant role in HCC development and progression. Nevertheless, specific mechanisms have not been extensively studied, which hence offers significant potential and research value.

In the present study, the focus was placed on the association of GPCRs with HCC. The clinical and expression data of 595 HCC patients were obtained from TCGA and LIRI-JP databases, and the focus was put on GPCR-related gene expression with the assistance of GPCR gene sets downloaded from MsigDB. LASSO and multivariant Cox regression analyses were followed by the identification of eight GPCR-related genes and the establishment of a GPCR-related risk score. Among these eight genes, NLRP6 was the only gene whose expression level was negatively related to the risk score. HCC patients were categorized into groups with high and low risks. Patients in the high-risk group showed a significantly worse prognosis. Differential expression analyses were performed, and significant differences in cell proliferation and differentiation, cell membrane channel activity, and metabolism were found. This conclusion further confirmed the effectiveness of the risk score model. PPI mechanisms were further explored. Hub genes and miRNA-target gene regulatory networks were constructed to see protein interactions. Five miRNAs including miR-155-5p, miR-135a-5p, miR-494-3p, miR-34a-5p and miR-410-3p were predicted as potentially regulating miRNAs, of which four [40,41] (miR-155-5p, miR-135a-5p, miR-494-3p and miR-34a-5p) had already proved to act as regulators in HCC. In addition, miR-410-3p was demonstrated to promote or suppress tumor progression in prostate [42] and breast [43] as well. This further validated the accuracy of the risk model
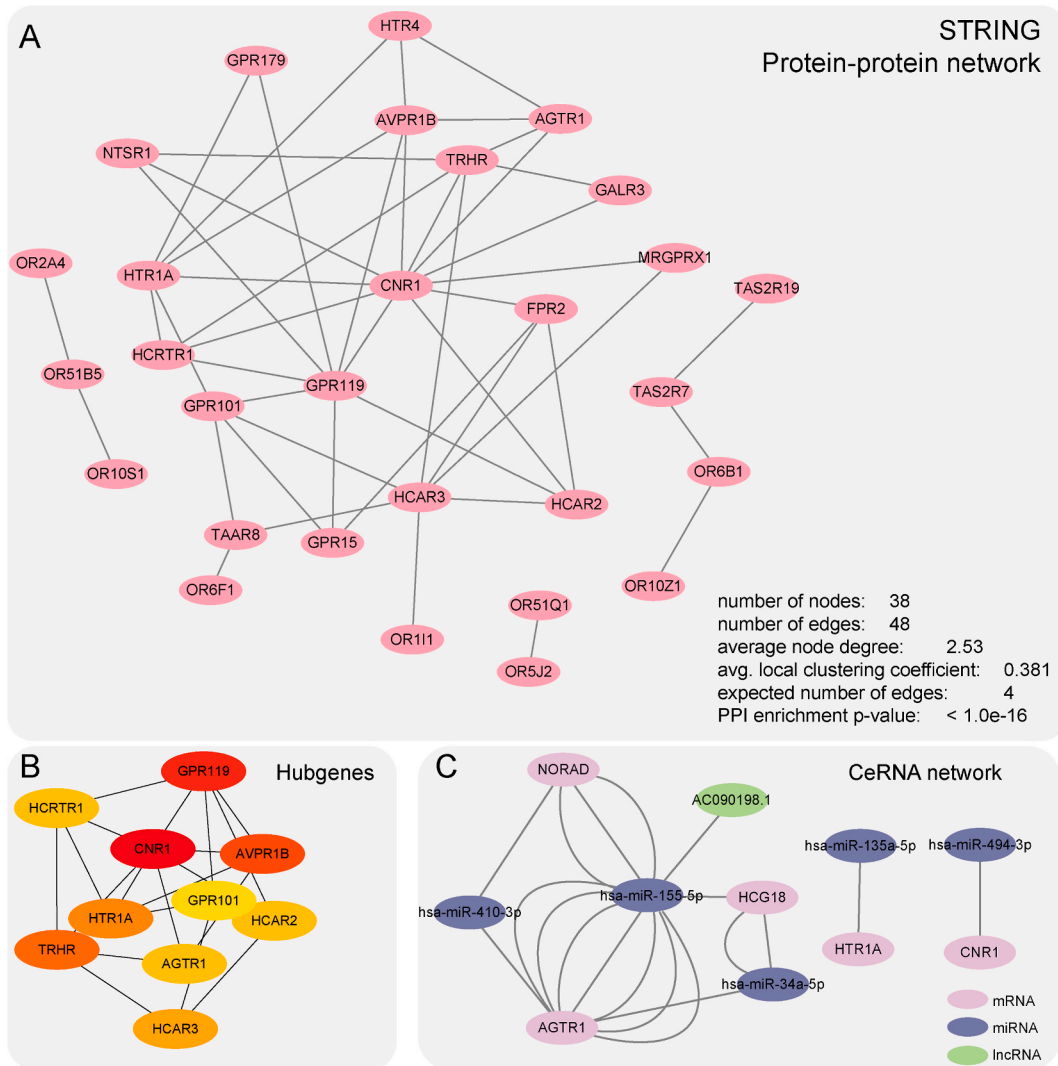
Fig. 6. Analysis of PPI regulatory network. (A) PPI regulatory network with specific information on its nodes, connecting lines and all sub-networks. (B) Calculation of hub gene regulatory network on the basis of CytoHubba. (C) Prediction of miRNA-hub gene regulatory network using the mirTarbase database.

indirectly. Immune infiltration level was evaluated, and the number of immune and stromal cells was found to be lower in the high-risk group. The high-risk group exhibited lower TIDE scores as well. Together, these suggested that patients in the high-risk group tended to respond to immunotherapy. The sensitivity of common HCC treatment drugs was evaluated. BIRB.0796 (p38 mitogen-activated protein kinase (MAPK) inhibitor) and ATRA showed higher sensitivity to the high-risk group of patients. However, AZD8055 (mammalian target of rapamycin (mTOR) inhibitor), EHT.1864 (Ras-related C3 botulinum toxin substrate (Rac1) inhibitor), PF.4708671 (ribosomal protein S6 kinase beta-1 (S6K1) inhibitor), and GW.441756 (tyrosine kinase-A (TrkA) inhibitor) demonstrated higher sensitivity to the low-risk group of patients. Finally, a clinical prediction model on the basis of GPCR-related risk scores was established, with excellent predictive power for the OS of patients with HCC.

Subsequently, in-depth research was conducted on eight genes in the predictive model. It was confirmed that six of the eight genes played a part in the occurrence, development, immune regulation or prognosis prediction of HCC. Also called CXCR, ACKR3 mainly serves as a scavenger receptor for CXCL12 [44]. Research has shown that CXCR7 overexpression was linked to the differentiation [45] and proliferation of HCC, and regulated the expression of vascular endothelial growth factor A (VEGFA) and galectin-3 to result in tumor angiogenesis, cell invasiveness, as well as metastasis [46,47]. Additionally, ACKR3 controlled the secretion of various in-flammatory factors and induced immune escape by regulating M2 macrophage migration in HCC [47]. Primarily expressed on the surface of eosinophils, CCR3 binds and responds to CCL11, CCL24 and CCL26, respectively [48]. It was observed that CCL26 showed a strong relationship with HCC proliferation, migration, invasion and angiogenesis [49], and CCL24 caused metastasis and neo-vascularization through the RhoB-VEGFA-VEGFR2 pathway and demonstrated a poor prognosis in HCC [50]. CCR7 mainly binds to
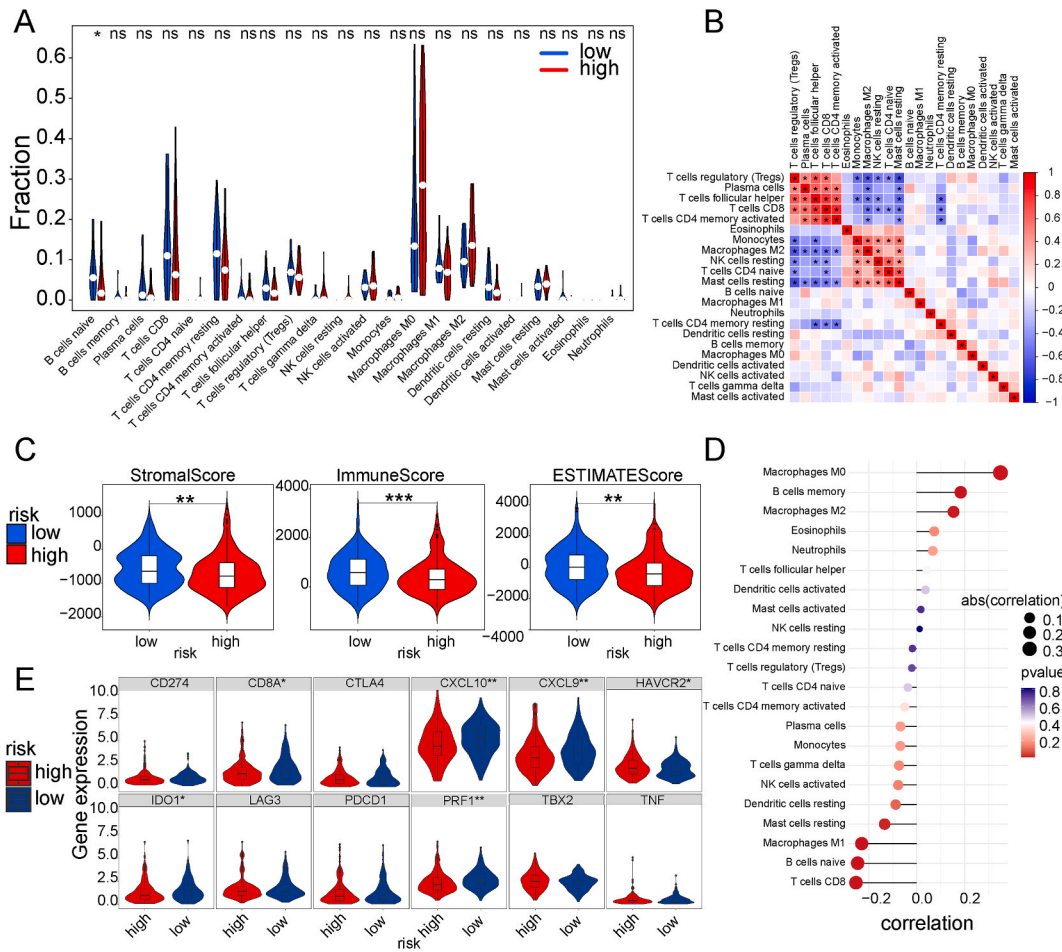
Fig. 7. Relationships between GPCR-related risk scores with different infiltration levels of immune cells. (A) Analysis of differences in the levels of 22 different immune cell infiltrates between both groups. (B) Panoramic analysis of immune cell infiltration and immune cell correlation analysis in the LIHC dataset. (C) Differences in stromal cells and ESTIMATE and immune scores between both groups. (D) Bar chart of the correlation analysis of GPCR-related risk scores with immune cell infiltration. (E) Differential expression analysis of different immune checkpoint genes between both subgroups (*P < 0.05, **P < 0.01 and ***P < 0.001).

CCL19 and CCL21 [51], whose axis often recruits regulatory T cells and tumor-infiltrating lymphocytes into the tumor niche and contributes to the improvement of prognosis [51]. The research results of CCR7 in HCC signified that CCR7 facilitated the progression of EMT, enhanced the invasion and proliferation of tumor cells, and demonstrated a relationship with lymphatic and intrahepatic dissemination [52,53]. It also increased levels of IL-10 and transforming growth factor-β1 (TGF-β1), decreased levels of IL-12 and interferon-gamma (IFN-γ), and played a role in shaping the tumor microenvironment [53]. FZD5 (Frizzled-5) belongs to one of the Frizzled receptor subtypes, namely wingless (Wnt) receptors, mediates the Wnt/β-catenin signaling pathway, activates liver cancer stem cells, and facilitates the progression [54] and metastasis of HCC [55]. HCAR1 is also called HCA1 or GPR81 and is viewed as a lactate receptor. It has been found that HCAR1 is overexpressed in HCC, and regulates angiogenesis and growth induced by tumor lactate [56,57]. NLRP6, a novel member of the nucleotide binding domain and leucine-rich repeat-containing (NLR) family, shows abundant expression in the liver and intestine and plays an essential role in regulating inflammation and shaping intestine microbiota [58]. It is demonstrated that NLRP6 drives the progression of liver diseases by causing dysbiosis of the intestine, and its expression level is strongly related to the prognosis of HCC by regulating the progress of pyroptosis [59,60]. GRM8 modulates glutamatergic and gamma-aminobutyric acid (GABA) neurotransmission, and HTR5A belongs to the 5-HT receptor family and is deeply involved in regulating the nervous system [61,62].

Most of the GPCRs included in the risk score model used in this study are either FDA-approved drug targets or drug targets in the phase of clinical trials. Small molecule inhibitors of ACKR3 were manufactured, including CCX771, CCX754 and CCX733 [63], among which the former two had already shown the capability of reducing nearly half of colorectal carcinoma lung metastases in vivo [64]. Maraviroc, including CCR5 and CCR3 antagonists, has been approved for the treatment of human immunodeficiency virus (HIV) infection [65]. CCR3 antagonist GW766994 showed safety and efficacy in asthma and eosinophilic bronchitis [66]. HTR5A antagonist SB-699551 has been proven to reduce the survival of breast tumor-initiating cells [67]. UCSF678, an arrestin-biased partial agonist,
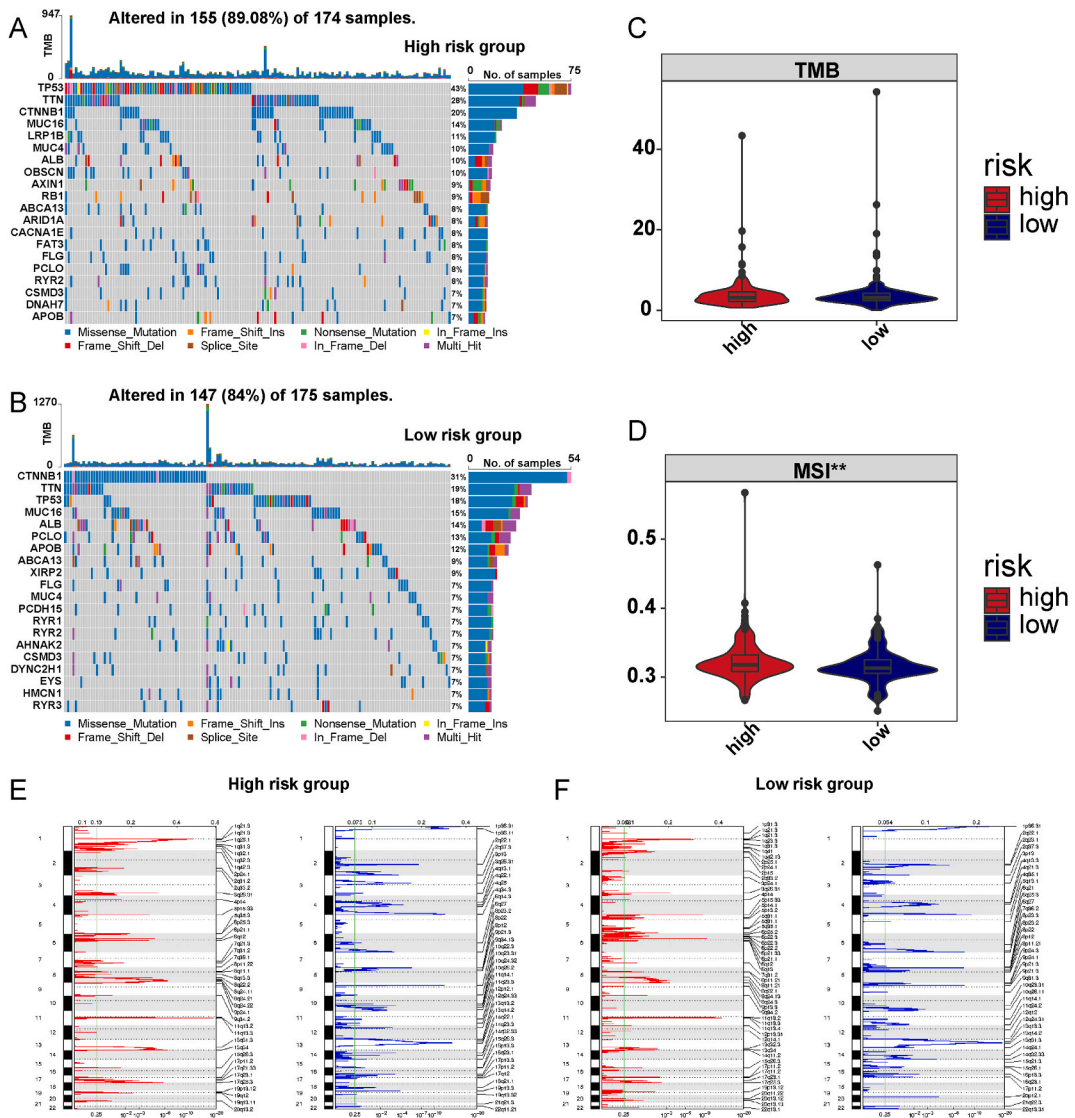
Fig. 8. Impact of GPCR-related risk score groupings on immunotherapy and genetic variation in patients with HCC. (A–B) Common tumorigenic driver gene mutation profiles of patients in both groups. The information on the mutation of genes in samples is illustrated in the waterfall plot, in which a variety of colors indicate different types of mutation; the mutational load is denoted by the vignettes above the legend. (C–D) Differences in TMB and MSI levels between patients in both groups; the high-risk group has significantly higher TMB and MSI levels than the low-risk one. (E–F) Copy number levels of genes in patients in both groups; red represents genes with a significant increase in copy number and blue stands for genes with a significant decrease in copy number; more copy number amplification and missing fragments are seen in the low-risk group (*P < 0.05, **P < 0.01 and ***P < 0.001). (For interpretation of the references to color in this figure legend, the reader is referred to the Web version of this article.)

was developed with a deeper understanding of the HTR5A structure. MSOP, microtubule-associated protein 4 (MAP4), (RS)-α-Cyclopropyl-4-phosphonophenylglycine (CPPG), UBP111 and LY341495 were manufactured as GRM8 antagonists recently. The crystal structure of CCR7 was elucidated. Thiazole-dioxide, thiadiazole-dioxide or cyclobutene-dione motifs are crucial for interaction with a conservative transmembrane helix 7-helix 8 (TM7-H8) protein patch in the binding site of Gi protein in chemokine receptors like CCR7 [68].

Some limitations exist in this study. Firstly, validation and training datasets had no large sample sizes, which may limit the statistical power of data analysis. Secondly, it is necessary to conduct extra experimental validations to expound the mechanisms of DEGs identified. Further studies in diverse populations or settings would be beneficial to validating and extending the scope of the research results.

It must be admitted that GPCRs in oncology are a relatively new topic and many underlying mechanisms remain unclear and need much further exploration compared with GPCRs in metabolic and physical disorders, as well as infectious diseases. Currently, some drugs for upstream or downstream targets have already been from GPCRs although not many GPCR-targeted drugs are directly used for
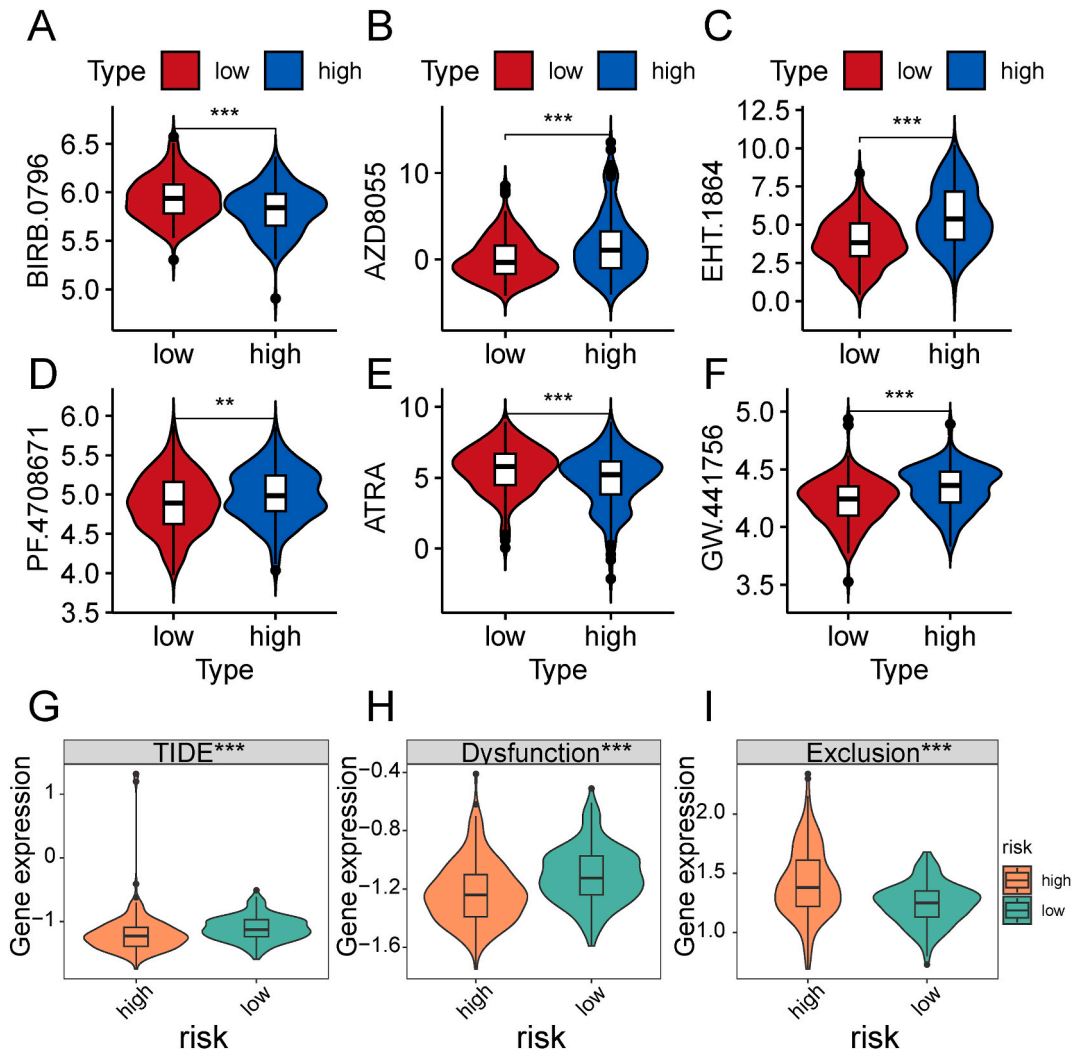
Fig. 9. Drug sensitivity analysis of patients in both groups in the GPCR-associated risk score model. (A–F) Top six drugs in terms of the P value of IC50 based on the Wilcox test between both groups; they are all less sensitive in the high-risk group. (G–I) Differences in TIDE, dysfunction and exclusive scores between both groups; this suggests the possibility that the high-risk group shows better responsiveness to immunotherapy (*P < 0.05, **P < 0.01 and ***P < 0.001).

antitumor therapy [69]. New avenues for the discovery of GPCR drugs have appeared thanks to recent advancements in receptor pharmacology, biotechnological innovations and breakthroughs in structural biology. Therefore, investigating the relationship between GPCRs and HCC further provides insights into both GPCR and GPCR downstream targets, which thus expands the repertoire for future HCC treatments.

Ethics statement

All data used in the study was obtained from public databases, hence, ethics approval and informed consent were not required.

Consent to participate

Not applicable.

Consent for publication

The authors declare that they agree to submit the article for publication.
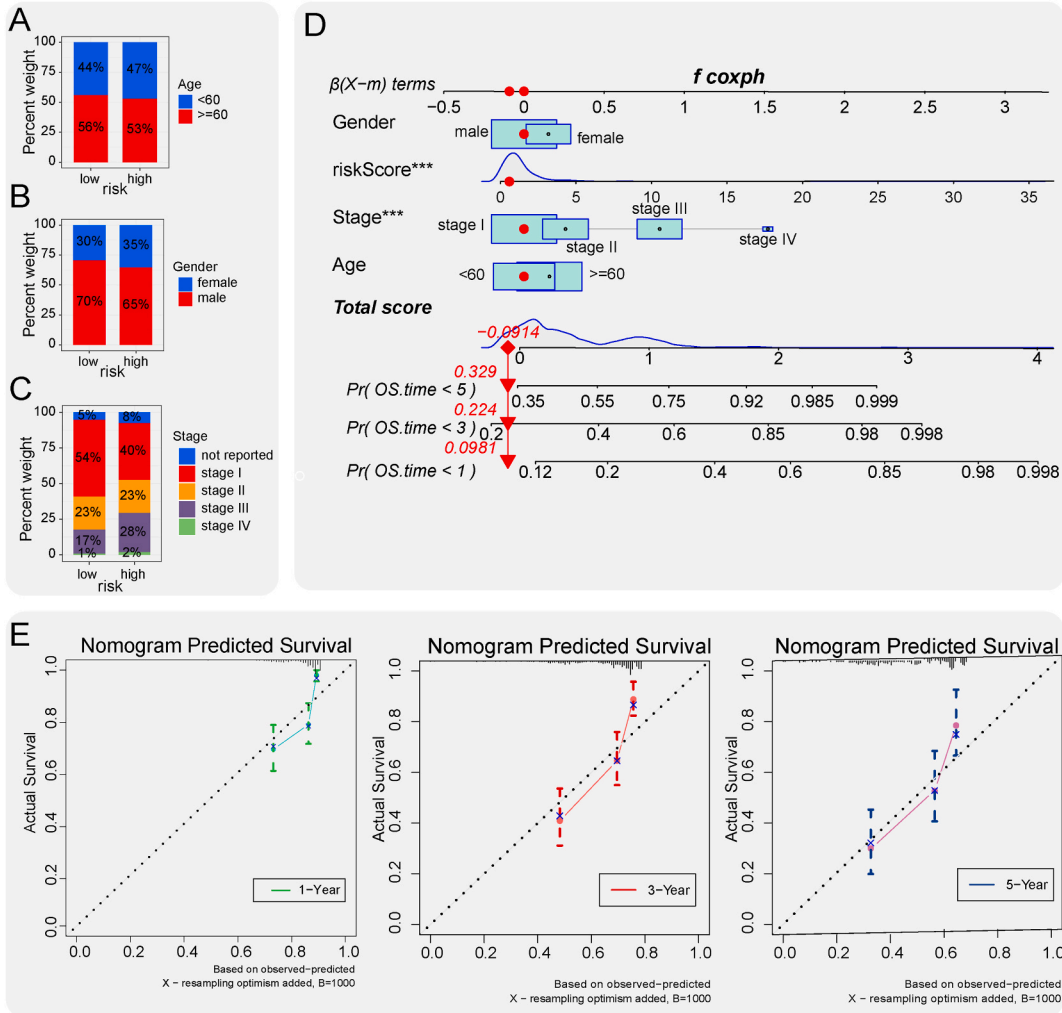
Fig. 10. Predictive power analysis of GPCR-related risk scores on the prognosis of patients with HCC. (A–C) Superimposed histograms showing the proportion of gender, age and stage among patients in both groups. Both groups are similar in the proportion of age and gender, and the low-risk group has significantly more early-stage patients than the high-risk one. (D) Nomogram of a clinical prediction model on the basis of GPCR-related risk scores in combination with clinicopathological characteristics. (E) Calibration curve of the nomogram; horizontal and vertical coordinates are the nomogram-predicted and actual observed survival statuses, respectively. Curves show that the nomogram model has good predictive value at one, three and five years.

Funding

Data availability statement

The names of the public repositories and their relevant accession links are detailed in the Materials and Methods section.

CRediT authorship contribution statement

Yuxin Wang: Writing – original draft, Methodology, Investigation, Formal analysis, Data curation, Conceptualization. **Bao Jin:** Supervision, Methodology, Investigation. **Xiangan Wu:** Visualization, Methodology, Formal analysis. **Jiali Xing:** Visualization, Validation, Methodology. **Baoluhe Zhang:** Validation, Supervision, Investigation. **Xiaokun Chen:** Writing – review & editing, Validation, Formal analysis. **Xiao Liu:** Writing – review & editing, Validation, Supervision. **Xueshuai Wan:** Writing – review & editing, Visualization, Validation. **Shunda Du:** Writing – review & editing, Validation, Funding acquisition, Conceptualization.

Declaration of competing interest

The authors declare that they have no known competing financial interests or personal relationships that could have appeared to influence the work reported in this paper.

Abbreviations

AUC	Area Under the Curves
ACKR3	Atypical Chemokine Receptor 3
BP	Biological Process
CCR3	C–C Chemokine Receptor Type 3
CCR7	C–C Chemokine Receptor Type 7
CNV	Copy Number Alteration
DEG	Differentially Expressed Gene
EMT	Epithelial–Mesenchymal Transition
ESTIMATE	Estimation of Stromal and Immune Cells in Malignant Tumor Tissues Using Expression Data
FDA	Food and Drug Administration
FDR	False Discovery Rate
FPKM	Fragments Per Kilobase Million
FZD5	Frizzled Class Receptor 5
GDSC	Genomics of Drug Sensitivity in Cancer
GO	Gene Ontology
GPCR	G Protein-Coupled Receptor
GSEA	Gene Set Enrichment Analysis
GISTIC	Genomic Identification of Significant Targets in Cancer
HAR1	Hydroxycarboxylic Acid Receptor 1
HCC	Hepatocellular Carcinoma
HTR5A	5-Hydroxytryptamine Receptor 5A
ICB	Immune Checkpoint Blockade
IL-6	Interleukin-6
KEGG	Kyoto Encyclopedia of Genes and Genomes
LIRI-JP	Liver Hepatocellular Carcinoma-Japan
MF	Molecular Function
MSI	Microsatellite Instability
MSigDB	Molecular Signatures Database
PPI	Protein-Protein Interaction
ROC	Receiver Operating Characteristic
SNP	Single Nucleotide Polymorphism
TCGA	The Cancer Genome Atlas
TIDE	Tumor Immune Dysfunction and Exclusion
TMB	Tumor Mutational Burden
TNM	Tumor Node Metastasis
TPM	Transcripts Per Million

References

[1] H. Sung, J. Ferlay, R.L. Siegel, et al., Global cancer statistics 2020: GLOBOCAN estimates of incidence and mortality worldwide for 36 cancers in 185 Countries, CA Cancer J Clin 71 (3) (2021) 209–249.

[2] A.B. EL-Khoueiry, B. Sangro, T. Yau, et al., Nivolumab in patients with advanced hepatocellular carcinoma (CheckMate 040): an open-label, non-comparative, phase 1/2 dose escalation and expansion trial, Lancet 389 (10088) (2017) 2492–2502.

[3] T. Yau, C. Hsu, T.Y. Kim, et al., Nivolumab in advanced hepatocellular carcinoma: sorafenib-experienced Asian cohort analysis, J. Hepatol. 71 (3) (2019) 543–552.

[4] F. Finkelmeier, C. Czauderna, L. Perkhofer, et al., Feasibility and safety of nivolumab in advanced hepatocellular carcinoma: real-life experience from three German centers, J. Cancer Res. Clin. Oncol. 145 (1) (2019) 253–259.

[5] C.T. Yeh, K.H. Liang, C.C. Lin, et al., A single nucleotide polymorphism on the GALNT14 gene as an effective predictor of response to chemotherapy in advanced hepatocellular carcinoma, Int. J. Cancer 134 (5) (2014) 1214–1224.

[6] D.M. Rosenbaum, S.G. Rasmussen, B.K. Kobilka, The structure and function of G-protein-coupled receptors, Nature 459 (7245) (2009) 356–363.

[7] A.S. Hauser, M.M. Attwood, M. Rask-Andersen, et al., Trends in GPCR drug discovery: new agents, targets and indications, Nat. Rev. Drug Discov. 16 (12) (2017) 829–842.

[8] P.A. Insel, K. Sriram, M.W. Gorr, et al., GPCRomics: an approach to discover GPCR drug targets, Trends Pharmacol. Sci. 40 (6) (2019) 378–387.

[9] M. O'Hayre, J. Vazquez-Prado, I. Kufareva, et al., The emerging mutational landscape of G proteins and G-protein-coupled receptors in cancer, Nat. Rev. Cancer 13 (6) (2013) 412–424.

[10] Z. Kan, B.S. Jaiswal, J. Stinson, et al., Diverse somatic mutation patterns and pathway alterations in human cancers, Nature 466 (7308) (2010) 869–873.
[11] M. O'Hayre, M.S. Degese, J.S. Gutkind, Novel insights into G protein and G protein-coupled receptor signaling in cancer, Curr. Opin. Cell Biol. 27 (2014) 126–135.
[12] R. Lappano, M. Maggiolini, G protein-coupled receptors: novel targets for drug discovery in cancer, Nat. Rev. Drug Discov. 10 (1) (2011) 47–60.
[13] S. Li, S. Huang, S.B. Peng, Overexpression of G protein-coupled receptors in cancer cells: involvement in tumor progression, Int. J. Oncol. 27 (5) (2005) 1329–1339.
[14] S.A. Forbes, N. Bindal, S. Bamford, et al., COSMIC: mining complete cancer genomes in the Catalogue of Somatic Mutations in Cancer, Nucleic Acids Res. 39 (Database issue) (2011) D945–D950.
[15] Z. Zhang, C. Qin, Y. Wu, et al., CCR9 as a prognostic marker and therapeutic target in hepatocellular carcinoma, Oncol. Rep. 31 (4) (2014) 1629–1636.
[16] Q. Gao, Y.J. Zhao, X.Y. Wang, et al., CXCR6 upregulation contributes to a proinflammatory tumor microenvironment that drives metastasis and poor patient outcomes in hepatocellular carcinoma, Cancer Res. 72 (14) (2012) 3546–3556.
[17] F. Liu, C. Zhu, X. Huang, et al., A low level of GPR37 is associated with human hepatocellular carcinoma progression and poor patient survival, Pathol. Res. Pract. 210 (12) (2014) 885–892.
[18] Q. Ding, Y. Xia, S. Ding, et al., An alternatively spliced variant of CXCR3 mediates the metastasis of CD133+ liver cancer cells induced by CXCL9, Oncotarget 7 (12) (2016) 14405–14414.
[19] Z. Liu, L. Yang, J. Xu, et al., Enhanced expression and clinical significance of chemokine receptor CXCR2 in hepatocellular carcinoma, J. Surg. Res. 166 (2) (2011) 241–246.
[20] K. Zheng, H.Y. Li, X.L. Su, et al., Chemokine receptor CXCR7 regulates the invasion, angiogenesis and tumor growth of human hepatocellular carcinoma cells, J. Exp. Clin. Cancer Res. 29 (1) (2010) 31.
[21] D.M. Kuang, Q. Zhao, Y. Wu, et al., Peritumoral neutrophils link inflammatory response to disease progression by fostering angiogenesis in hepatocellular carcinoma, J. Hepatol. 54 (5) (2011) 948–955.
[22] F. Deshayes, C. Nahmias, Angiotensin receptors: a new role in cancer? Trends Endocrinol Metab 16 (7) (2005) 293–299.
[23] Z. Ma, D. Guo, Q. Wang, et al., Lgr5-mediated p53 Repression through PDCD5 leads to doxorubicin resistance in Hepatocellular Carcinoma, Theranostics 9 (10) (2019) 2967–2983.
[24] T. Wei, W. Chen, L. Wen, et al., G protein-coupled estrogen receptor deficiency accelerates liver tumorigenesis by enhancing inflammation and fibrosis, Cancer Lett. 382 (2) (2016) 195–202.
[25] Y. Gao, M. You, J. Fu, et al., Intratumoral stem-like CCR4+ regulatory T cells orchestrate the immunosuppressive microenvironment in HCC associated with hepatitis B, J. Hepatol. 76 (1) (2022) 148–159.
[26] M.D. Wilkerson, D.N. Hayes, ConsensusClusterPlus: a class discovery tool with confidence assessments and item tracking, Bioinformatics 26 (12) (2010) 1572–1573.
[27] W. Cai, M. Van Der Laan, Nonparametric bootstrap inference for the targeted highly adaptive least absolute shrinkage and selection operator (LASSO) estimator, Int. J. Biostat. 16 (2) (2020) 1–34.
[28] M.I. Love, W. Huber, S. Anders, Moderated estimation of fold change and dispersion for RNA-seq data with DESeq2, Genome Biol. 15 (12) (2014) 550.
[29] M. Ashburner, C.A. Ball, J.A. Blake, et al., Gene ontology: tool for the unification of biology. The Gene Ontology Consortium, Nat. Genet. 25 (1) (2000) 25–29.
[30] H. Ogata, S. Goto, K. Sato, et al., KEGG: kyoto Encyclopedia of genes and genomes, Nucleic Acids Res. 27 (1) (1999) 29–34.
[31] G. Yu, L.G. Wang, Y. Han, et al., clusterProfiler: an R package for comparing biological themes among gene clusters, OMICS 16 (5) (2012) 284–287.
[32] A. Subramanian, P. Tamayo, V.K. Mootha, et al., Gene set enrichment analysis: a knowledge-based approach for interpreting genome-wide expression profiles, Proc Natl Acad Sci U S A 102 (43) (2005) 15545–15550.
[33] D. Szklarczyk, A.L. Gable, K.C. Nastou, et al., The STRING database in 2021: customizable protein-protein networks, and functional characterization of user-uploaded gene/measurement sets, Nucleic Acids Res. 49 (D1) (2021) D605–D612.
[34] K. Yoshihara, M. Shahmoradgoli, E. Martinez, et al., Inferring tumour purity and stromal and immune cell admixture from expression data, Nat. Commun. 4 (2013) 2612.
[35] A.M. Newman, C.L. Liu, M.R. Green, et al., Robust enumeration of cell subsets from tissue expression profiles, Nat. Methods 12 (5) (2015) 453–457.
[36] J. Fu, K. Li, W. Zhang, et al., Large-scale public data reuse to model immunotherapy response and resistance, Genome Med. 12 (1) (2020) 21.
[37] W. Yang, J. Soares, P. Greninger, et al., Genomics of Drug Sensitivity in Cancer (GDSC): a resource for therapeutic biomarker discovery in cancer cells, Nucleic Acids Res. 41 (Database issue) (2013) D955–D961.
[38] P. Geeleher, N. Cox, R.S. Huang, pRRophetic: an R package for prediction of clinical chemotherapeutic response from tumor gene expression levels, PLoS One 9 (9) (2014) e107468.
[39] P. Blanche, J.F. Dartigues, H. Jacqmin-Gadda, Estimating and comparing time-dependent areas under receiver operating characteristic curves for censored event times with competing risks, Stat. Med. 32 (30) (2013) 5381–5397.
[40] Y. Li, Y. Zhang, S. Zhang, et al., circRNA circARNT2 suppressed the sensitivity of hepatocellular carcinoma cells to cisplatin by targeting the miR-155-5p/PDK1 Axis, Mol. Ther. Nucleic Acids 23 (2021) 244–254.
[41] N. Van Renne, A.A. Roca Suarez, F.H.T. Duong, et al., miR-135a-5p-mediated downregulation of protein tyrosine phosphatase receptor delta is a candidate driver of HCV-associated hepatocarcinogenesis, Gut 67 (5) (2018) 953–962.
[42] Y. Zhang, D. Zhang, J. Lv, et al., miR-410-3p promotes prostate cancer progression via regulating PTEN/AKT/mTOR signaling pathway, Biochem. Biophys. Res. Commun. 503 (4) (2018) 2459–2465.
[43] Y.F. Zhang, Y. Yu, W.Z. Song, et al., miR-410-3p suppresses breast cancer progression by targeting Snail, Oncol. Rep. 36 (1) (2016) 480–486.
[44] J.M. Burns, B.C. Summers, Y. Wang, et al., A novel chemokine receptor for SDF-1 and I-TAC involved in cell survival, cell adhesion, and tumor development, J. Exp. Med. 203 (9) (2006) 2201–2213.
[45] T.C. Xue, Q.A. Jia, Y. Bu, et al., CXCR7 correlates with the differentiation of hepatocellular carcinoma and suppresses HNF4alpha expression through the ERK pathway, Oncol. Rep. 32 (6) (2014) 2387–2396.
[46] L. Lin, M.M. Han, F. Wang, et al., CXCR7 stimulates MAPK signaling to regulate hepatocellular carcinoma progression, Cell Death Dis. 5 (10) (2014) e1488.
[47] Y. Chen, F. Teng, G. Wang, et al., Overexpression of CXCR7 induces angiogenic capacity of human hepatocellular carcinoma cells via the AKT signaling pathway, Oncol. Rep. 36 (4) (2016) 2275–2281.
[48] C.J. Millard, J.P. Ludeman, M. Canals, et al., Structural basis of receptor sulfotyrosine recognition by a CC chemokine: the N-terminal region of CCR3 bound to CCL11/eotaxin-1, Structure 22 (11) (2014) 1571–1581.
[49] Z.Y. Lin, Y.H. Chuang, W.L. Chuang, Cancer-associated fibroblasts up-regulate CCL2, CCL26, IL6 and LOXL2 genes related to promotion of cancer progression in hepatocellular carcinoma cells, Biomed. Pharmacother. 66 (7) (2012) 525–529.
[50] L. Jin, W.R. Liu, M.X. Tian, et al., CCL24 contributes to HCC malignancy via RhoB- VEGFA-VEGFR2 angiogenesis pathway and indicates poor prognosis, Oncotarget 8 (3) (2017) 5135–5148.
[51] P. Correale, M.S. Rotundo, C. Botta, et al., Tumor infiltration by T lymphocytes expressing chemokine receptor 7 (CCR7) is predictive of favorable outcome in patients with advanced colorectal carcinoma, Clin. Cancer Res. 18 (3) (2012) 850–857.
[52] L. Yang, Y. Chang, P. Cao, CCR7 preservation via histone deacetylase inhibition promotes epithelial-mesenchymal transition of hepatocellular carcinoma cells, Exp. Cell Res. 371 (1) (2018) 231–237.
[53] C.C. Schimanski, R. Bahre, I. Gockel, et al., Chemokine receptor CCR7 enhances intrahepatic and lymphatic dissemination of human hepatocellular cancer, Oncol. Rep. 16 (1) (2006) 109–113.
[54] X. Liu, J. Qin, T. Gao, et al., YTHDF1 facilitates the progression of hepatocellular carcinoma by promoting FZD5 mRNA translation in an m6A-dependent manner, Mol. Ther. Nucleic Acids 22 (2020) 750–765.

[55] Q. Zhu, G. Lu, Z. Luo, et al., CircRNA circ_0067934 promotes tumor growth and metastasis in hepatocellular carcinoma through regulation of miR-1324/FZD5/Wnt/beta-catenin axis, Biochem. Biophys. Res. Commun. 497 (2) (2018) 626–632.
[56] V.L. Payen, E. Mina, V.F. Van Hee, et al., Monocarboxylate transporters in cancer, Mol Metab 33 (2020) 48–66.
[57] C.L. Roland, T. Arumugam, D. Deng, et al., Cell surface lactate receptor GPR81 is crucial for cancer cell survival, Cancer Res. 74 (18) (2014) 5301–5310.
[58] H. Hara, S.S. Seregin, D. Yang, et al., The NLRP6 inflammasome recognizes lipoteichoic acid and regulates gram-positive pathogen infection, Cell 175 (6) (2018) 1651–1664 e14.
[59] H. Wang, B. Zhang, Y. Shang, et al., A novel risk score model based on pyroptosis-related genes for predicting survival and immunogenic landscape in hepatocellular carcinoma, Aging (Albany NY) 15 (5) (2023) 1412–1444.
[60] X. Gao, W.X. Wang, X.L. Zhang, A novel pyroptosis risk model composed of NLRP6 effectively predicts the prognosis of hepatocellular carcinoma patients, Cancer Med. 12 (1) (2023) 808–823.
[61] A. Vaidya, S. Jain, A.K. Jain, et al., Metabotropic glutamate receptors: a review on prospectives and therapeutic aspects, Mini Rev. Med. Chem. 13 (13) (2013) 1967–1981.
[62] J. Raber, R.M. Duvoisin, Novel metabotropic glutamate receptor 4 and glutamate receptor 8 therapeutics for the treatment of anxiety, Expert Opin Investig Drugs 24 (4) (2015) 519–528.
[63] Y. Yang, J. Li, W. Lei, et al., CXCL12-CXCR4/CXCR7 Axis in cancer: from mechanisms to clinical applications, Int. J. Biol. Sci. 19 (11) (2023) 3341–3359.
[64] E. Guillemot, B. Karimdjee-Soilihi, E. Pradelli, et al., CXCR7 receptors facilitate the progression of colon carcinoma within lung not within liver, Br. J. Cancer 107 (12) (2012) 1944–1949.
[65] R. Horuk, Chemokine receptor antagonists: overcoming developmental hurdles, Nat. Rev. Drug Discov. 8 (1) (2009) 23–33.
[66] H. Neighbour, L.P. Boulet, C. Lemiere, et al., Safety and efficacy of an oral CCR3 antagonist in patients with asthma and eosinophilic bronchitis: a randomized, placebo-controlled clinical trial, Clin. Exp. Allergy 44 (4) (2014) 508–516.
[67] A. Levit Kaplan, R.T. Strachan, J.M. Braz, et al., Structure-based design of a chemical probe set for the 5-HT(5A) serotonin receptor, J. Med. Chem. 65 (5) (2022) 4201–4217.
[68] K. Jaeger, S. Bruenle, T. Weinert, et al., Structural basis for allosteric ligand recognition in the human CC chemokine receptor 7, Cell 178 (5) (2019) 1222–1230 e10.
[69] K. Sriram, P.A. Insel, G protein-coupled receptors as targets for approved drugs: how many targets and how many drugs? Mol. Pharmacol. 93 (4) (2018) 251–258.